EXCAVATION SEISMOLOGY

Duane E. Soiand, et al

Honeywell, Incorporated

Prepared for:

Advanced Research Projects Agency

December 1972

Security Classification

DOCUMENT CONTROL DATA - R & D

(Security classification of title, body of abstract and indexing annotation must be entered when the overall report is classified)

1 ORIGINATING ACTIVITY (Corporate author) Honeywell Inc. Systems and Research Center St. Paul, Minn. 55113	2a. REPORT SECURITY CLASSIFICATION Unclassified 2b. GROUP NA

3 REPORT TITLE

Excavation Seismology

4 DESCRIPTIVE NOTES (Type of report and inclusive dates)

Semiannual Technical Report 23 May 1972-22 November 1972

5 AUTHOR(S) (First name, middle initial, last name)

Duane E. Soland, Harold M. Mooney

6 REPORT DATE December 1972	7a. TOTAL NO. OF PAGES 66	7b. NO. OF REFS 8
8a CONTRACT OR GRANT NO H0220070 b. PROJECT NO ARPA Order No. 1579, Amend. 2 c Program Code No. 1F10 d	9a. ORIGINATOR'S REPORT NUMBER(S) F0154-TR1 9b. OTHER REPORT NO(S) (Any other numbers that may be assigned this report)	

10 DISTRIBUTION STATEMENT

11 SUPPLEMENTARY NOTES	12. SPONSORING MILITARY ACTIVITY Advanced Research Projects Agency Department of Defense Washington, D. C.

13 ABSTRACT

A portable prototype seismic/acoustic system has been developed. The system includes a pneumatically clamped borehole receiver and a down-hold spark source. Piezoelectric transducers and nonrepetitive sources, such as hammers can also be used with the system. The seismic signals are recorded directly on photographic film as a variable density. Seismic array configurations up to 512 elements can be recorded on one Polaroid film.

Ia

DD FORM 1 NOV 1473 REPLACES DD FORM 1473, 1 JAN 65, WHICH IS OBSOLETE FOR ARMY USE.

Security Classification

Security Classification

14 KEY WORDS	LINK A		LINK B		LINK C	
	ROLE	WT	ROLE	WT	ROLE	WT
RAPID EXCAVATION						
PORTABLE SEISMIC SYSTEM						
BOREHOLE RECEIVER						
VARIABLE DENSITY RECORDER						
UNDERWATER SPARK SOURCE						
SEISMIC ARRAYS						
REFLECTION SEISMOLOGY						
BEAMFORMING						
THREE-DIMENSIONAL METHOD						

F0154-TR1
2810-3004

December 1972

EXCAVATION SEISMOLOGY

Semiannual Technical Report

Bureau of Mines Contract No. H0220070

Sponsored by

Advanced Research Projects Agency
ARPA Order No. 1579, Amend. 2
Program Code No. 1F10

Duane E. Soland, Project Engineer 612/331-4141
Dr. Harold M. Mooney, Subcontract Principal Investigator 612/331-3137

Contract Effective Date: 23 May 1972
Expiration Date: 23 May 1973
Amount: $142,745

This research was supported by the Advanced Research Projects Agency of the Department of Defense and was monitored by the Bureau of Mines under Contract No. H0220070.

Honeywell Inc.
Systems and Research Center
Research Department
2345 Walnut Street
St. Paul, Minnesota 55113

IC

CONTENTS

ILLUSTRATIONS

TABLES

SECTION I

1.0 TECHNICAL REPORT SUMMARY

The feasibility of using seismic waves to detect discontinuities in rocks is well established. The capability to detect and map such discontinuities, whether from faulting, changes in rock type, voids, or abandoned mine workings, would be useful in deep underground excavation and mining operations.

At the present time, this capability exists for distances of only a few feet. The reasons are twofold:

(1) The ultrasonic frequencies used are absorbed too rapidly in the rock, and

(2) Unambiguous interpretation is made difficult by the presence of multiple wave arrivals.

The solution to the first problem is a more suitable seismic source. We have investigated, analytically and experimentally, the characteristics of several possible sources for use on the tunnel working face and wall surfaces and also in small diameter drill holes.

The lack of a suitable down-hole source led to the selection and development of an underwater spark source based on the electrohydraulic effect. Although this principle had been previously applied as a source for ocean acoustics and offshore seismic exploration, the electrode configurations, energy levels, and seismic pulse characteristics were not suitable for a portable, down-hole source. The device developed provides an estimated 12 joules acoustic output in a pulse of 30-100 microseconds duration.

Our approach to the problem of multiple arrivals is the use of seismic array techniques to separate the reflections and unwanted arrivals. Two methods, developed during a previous program, are to be verified and evaluated using field recorded data during the current program. These techniques are:

(1) Beamforming, which uses array signal processing to enhance arrivals from specific directions, and

(2) A three-dimensional CRT display where displayed intensity is proportional to the received seismic signal at a point in time and display spatial coordinates are proportional to array element spatial coordinates.

Both methods utilize crossed array configurations which can be conveniently implemented in confined underground spaces with down-hole seismic source and receiver arrays.

To provide field data for evaluation of the array methods, a portable prototype seismic/acoustic system has been developed. Conventional seismic systems generally record on magnetic tape the signals received simultaneously on a large array of receivers for subsequent processing and display. In contrast, our system approach is to present the seismic signals as a variable intensity CRT display and record directly as density variations on Polaroid film. The film can be interpreted immediately in the field, or digitized for further processing.

The system includes a pneumatically clamped borehole receiver and the borehole spark source referred to above. Provision was also made for an optional pulsed piezoelectric transducer. Nonrepetitive sources, such as impacting hammers, can also be used with the system.

In operation, the single repetitive source and single receiver provide one array output signal at a time. Each signal is recorded on film and the receiver repositioned and the film advanced for the next record. In this way, an array consisting of as many as 512 elements can be recorded on a single 4x5 Polaroid film.

SECTION II

2.0 INTRODUCTION

The objectives of this program are to verify and evaluate two promising seismic array techniques for use in underground hard-rock excavations. The two array techniques to be evaluated are:

(1) A three-dimensional method of displaying the output signals from a two-dimensional array of transmitting sources and receivers to enable an operator to visually detect reflections from discontinuities within the probed rock volume; and

(2) A beamforming method developed in a previous study which employs sophisticated array signal processing to enhance reflections returned from specific directions.

The evaluation and comparison of these two techniques for detection and location of rock discontinuities are directed toward future applications of the ARPA Rock Mechanics and Rapid Excavation Program. Thus, we are primarily concerned with deep underground openings in crystalline rocks. Specifically, we would anticipate relatively few reflecting discontinuities, but those that did exist would be of primary interest: changes in rock type, altered zones, or faults. Since these features are also of interest for mining operations, successful development of an underground seismic mapping technique might also be expected to be useful in underground mining operations.

The underground use of seismic methods is viewed as complementary to exploratory drilling, rather than as a replacement. Although incapable of the accuracy provided by drilling, seismic methods can economically probe substantially larger volumes of rock. Discontinuities can be seismically mapped and the nature of the discontinuity determined from a single borehole, where multiple boreholes might otherwise be required.

Of critical importance to the rapid excavation application is the timeliness of the information provided by the seismic system. The value of the information is determined by the amount of advanced warning of changing geologic conditions ahead of the excavation working face. This requirement implies that the seismic system approach must be capable of being implemented in nearly real time and that the penetration depth be as large as possible.

The attenuation factor for seismic waves in rock is proportional to frequency. Thus, as greater penetration is required, lower frequencies must be used. However, since the ability to resolve range differences depends on the wavelengths employed, there will be some transmitted pulse spectrum which provides the best compromise between resolution and penetration.

A significant part of the present program is concerned with seismic source development and evaluation. In addition to the frequency content of the seismic pulse, other source considerations include pulse duration, energy, repeatability, method of coupling to the rock, and portability.

A range of at least 50 meters is desirable for use in rapid excavation applications. Because of frequency-dependent attenuation, a significant fraction of the transmitted pulse energy should be contained below 5-10 KHz.

Moreover, to achieve a range resolution of one meter for a typical hard-rock seismic velocity of 5000 meters/second, the pulse duration should be no more than one or two hundred microseconds.

The seismic pulse can be applied either to the surface of the rock or to the interior of a borehole. Problems arising with a surface source include.

(1) That of coupling to a rough and uneven surface,

(2) The possibility of near-surface fractures caused by blasting or rock stress release, which would interfere with propagation of the seismic pulse, and

(3) Generation of interfering Rayleigh surface waves.

The use of a borehole source would alleviate these problems, but would require the added expense of drilling the hole and may introduce further complications.

At the start of the current phase of the program, there were a number of surface-type sources available from which to choose, including hammers and other impact sources as well as piezoelectric transducers. Consequently, effort was directed toward developing a suitable down-hole source and evaluation of existing surface sources. An additional requirement was that the hole diameter required for the source be no more than about 1-1/2 inches, to minimize drilling cost.

Similar considerations apply to the use of borehole receivers. The same problems arise in the use of surface-emplaced receivers as for surface sources. Hydrophones or pressure sensors in a water-filled hole are an

alternative possibility, but the presence of the fluid in the hole allows other wave modes to propagate along the hole. These waves would tend to interfere with or obscure the desired reflections. Thus, a second goal for this program phase has been the development of a receiving sensor which can be readily clamped to the wall of a small diameter borehole.

A third goal for this phase has been the development of an optical recorder which displays the received signals as a CRT intensity-modulation and provides a variable density film record of the seismic array output. The three-dimensional display can be viewed directly from the variable density negative, which can also be digitized for beamforming purposes. Usually, in seismic recording systems, magnetic tape is used as an intermediate storage medium. However, for simplicity and minimum cost, and because of the eventual need for real-time viewing, the intensity-modulated CRT with photographic film recording was chosen.

Together, the seismic source, receiver, and CRT display-recorder constitute a relatively inexpensive, portable seismic array system for use in underground excavations. The addition of an optical viewer will allow near real-time field interpretation using the three-dimensional display method, and a computer module for beamforming can also be added, if desirable, at some future date.

SECTION III

3.0 SEISMIC ARRAY APPROACHES

The use of seismic source/receiver arrays offers several advantages over a single source and receiver combination for reflection seismology:

- Identification of particular wave types is enhanced.
- Reflected waves arriving from some particular direction can be enhanced relative to other interfering waves.
- Direction to a reflector can be determined.

Two distinctly different array concepts will be evaluated in an underground environment during the next phase of the program. These two approaches are:

(1) Beamforming or spatial filtering, and

(2) The "three-dimensional seismic method".

The application of beamforming to the hard rock excavation problem was investigated under a previous contract (Ref. 7), while the 3-D method is a new way to present seismic array data which has been recently developed by ESSO Production Research Company for conventional seismic exploration (Refs. 3, 8).

3.1 Array Configurations for Underground Applications

Regardless of the array concept used for processing and display of the data, a two-dimensional or planar array is required by the three-dimensional nature of the underground problem, if dip and strike angles of reflecting surface are desired. The ideal configuration would consist of a large square array of N^2 seismometers distributed on a flat surface (Fig. 3-1). This approach would, in general, be impractical for underground use because:

(1) A sufficiently large flat surface would probably not be available, and

(2) The cost of providing N^2 receiving elements would be prohibitive.

Alternatively, a single scanning receiver could be used with a repetitive source (Fig. 3-1), but the first objection would still be valid. The flatness requirement could be relaxed somewhat by measuring the displacement of each receiver position relative to a datum plane and providing appropriate time delays for each receiver output signal. However, this approach also seems impractical and costly.

An alternative is to use crossed linear arrays. Milder and Wells (Ref. 5) have described a crossed array consisting of a line array of receivers and a line array of transmitters for acoustical holography (Fig. 3-2a). With this configuration, only 2N transducers (N receivers and N transmitters) are required for the equivalent of a square array of N^2 receivers [the $(n, m)^{th}$ datum results from listening to the m^{th} transmitter with the n^{th} receiver].

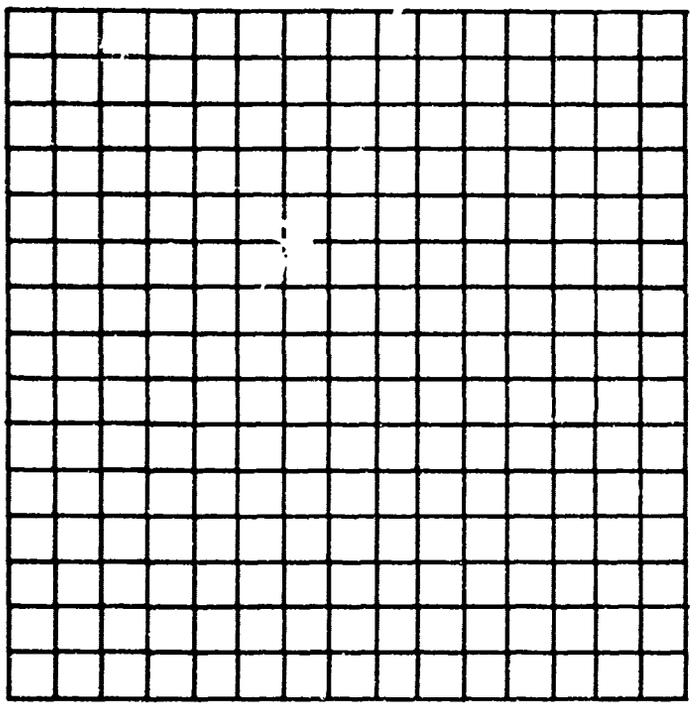

Figure 3-1. Square Array of N^2 Receivers

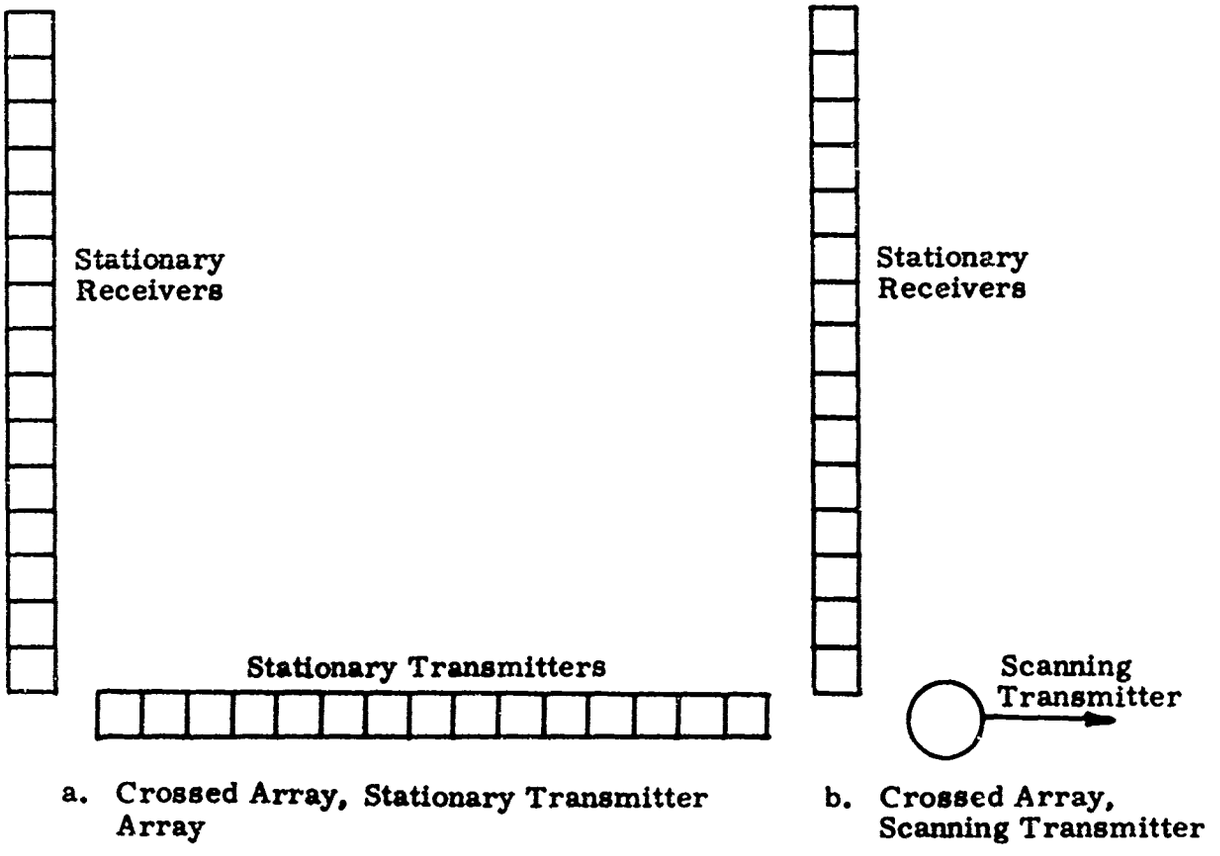

a. Crossed Array, Stationary Transmitter Array

b. Crossed Array, Scanning Transmitter

Figure 3-2. Alternatives to Square Array

This approach was also adopted for the 3-D method for seismic exploration (Ref. 8). There are several advantages of the crossed array technique for underground application. For example, perpendicular holes can be drilled in the rock for the two line arrays (Fig. 3-3). The inner surfaces of the holes will provide reasonably smooth, uniform surfaces for coupling the seismic energy into and out of the rock. The holes can be extended to any practical length D, so the size of the array (hence, angular resolution) is not restricted by the dimensions of the mine or tunnel opening. The holes can be drilled into the walls, floor, and/or roof parallel to the working face, but away from the face to minimize interference with excavation operations.

The crossed-array data can also be synthesized by:

(1) Using a single scanning transmitter with a stationary receiving array (Fig. 3-2b),

(2) Using a single scanning receiver with a stationary transmitter array, or

(3) Using a scanning receiver and a scanning transmitter.

This last approach for data generation has the advantages of simplicity, low cost, and ease of implementation, and has been selected for the evaluation phase of the program. It is also the slowest, so that we might anticipate one of the other approaches being more suitable for implementation in an operational system.

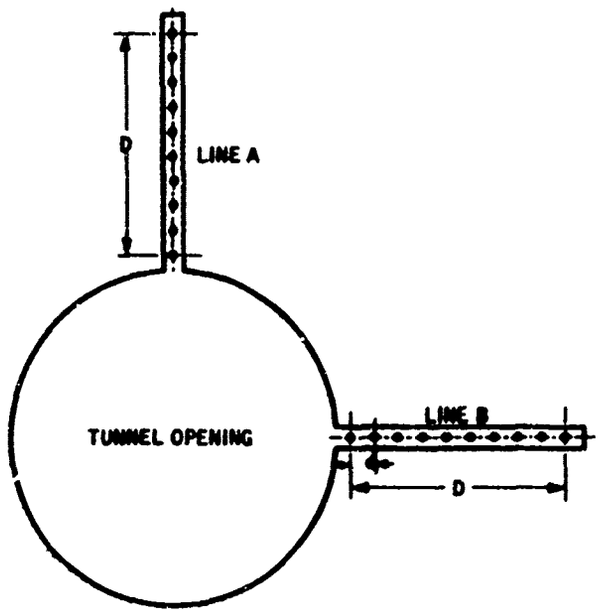

Figure 3-3. Crossed Array in Boreholes

A crossed-array configuration was also recommended for beamforming as a result of the previous study (Ref. 7). The configuration investigated there consisted of perpendicular line arrays of receivers, with a single transmitter at the intersection of the two lines. This configuration could be implemented with either stationary receiver arrays (Fig. 3-4a), or with a single scanning receiver and repetitive source. The outputs of each array were separately combined to form beams with good angular resolution in the two spatial coordinates normal to the array axis. The beamformer outputs for each line array were then cross-correlated with those of the other (Fig. 3-4b) to provide narrow beams in three spatial coordinates.

3.2 Beamforming Algorithms

The beamforming algorithms previously recommended for further field-scale investigation were as follows:

- Digital Multibeam Steering (DIMUS)
- DIMUS/Adaptive Null

These recommendations were based on simplicity of implementation and relative performance with respect to other possibilities which included:

(1) Delay-and-sum beamforming

(2) Weighted delay-and-sum beamforming

(3) Fan filtering

(4) Least-squares (Wiener) spatial filtering

(5) Adaptive beamforming

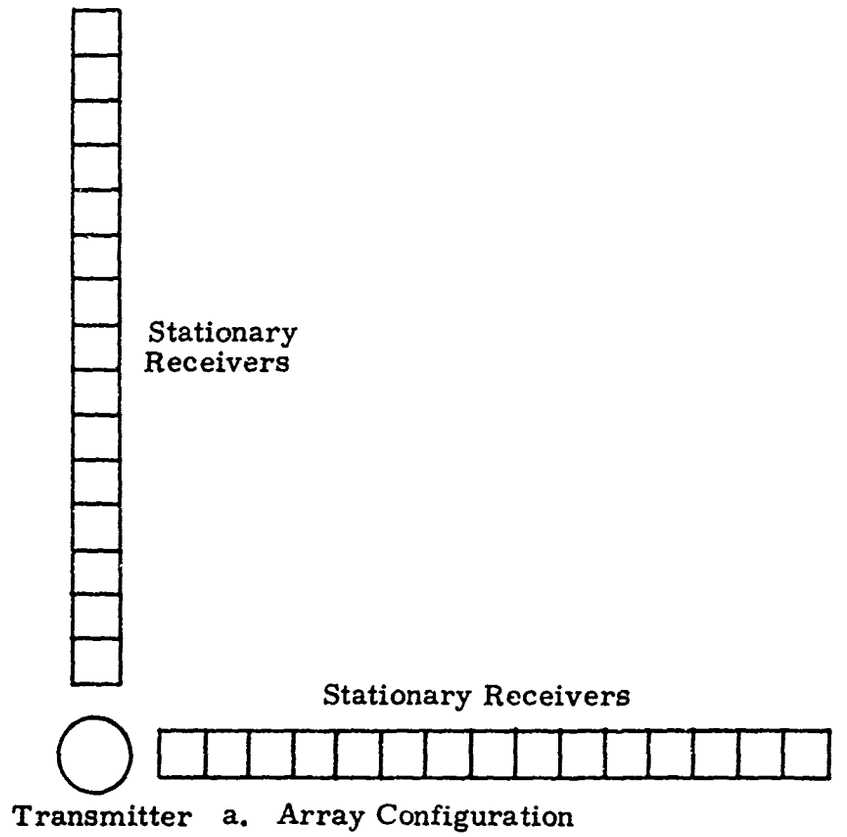

a. Array Configuration

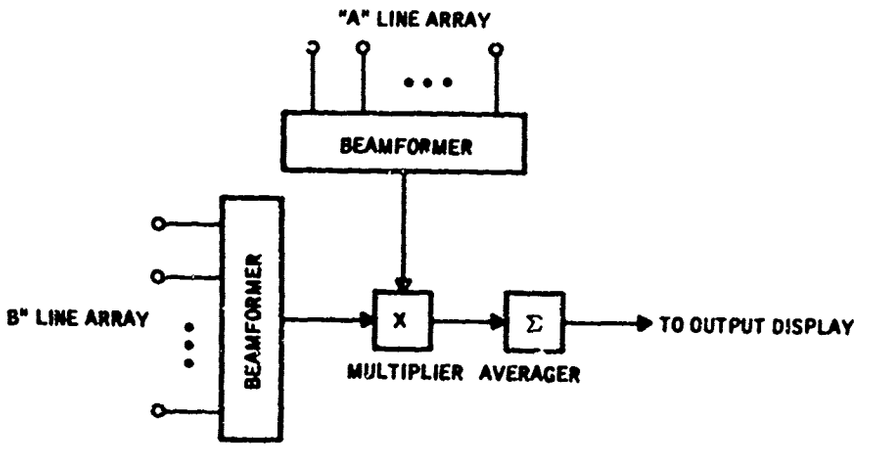

b. Crossed Correlation

Figure 3-4. Crossed Array for Beamforming

The DIMUS and DIMUS/Adaptive Null methods both employ hard clipping of the receiver outputs. That is, only the polarities of the signals are processed. Clipping provides several benefits and some adverse effects as well. Benefits include:

- Simpler implementation
- Insensitivity to amplitude variations
- Strong interferences are reduced, relative to small signals

Simpler implementation results from processing only the polarity bit. This reduces analog-to-digital conversion, data storage and digital processing requirements. Amplitude variations due to differences in source/receiver coupling to the rock across the array or variations in source output are unimportant and there is no need for AGC. On the other hand, disadvantages include the broadening of narrow pulses with tails (decrease of resolution), and the possibility of reducing strong signals relative to weak interferences. On balance, however, the advantages of hard clipping appear to outweigh the disadvantages.

3.2.1 The DIMUS Algorithm -- DIMUS beamforming consists of delay-and-sum beamforming on hard-clipped data:

$$b(n) = \sum_k \text{sgn}\,[s_k(n-m_k)]$$

where

$$\text{sgn}(z) = \begin{cases} +1, & z \geq 0 \\ -1, & z < 0 \end{cases},$$

and $s_k(n)$ is the amplitude of the signal sensed at the k^{th} receiver at the n^{th} sample instant after transmission of a pulse by the source. The integer m_k is the delay applied to the k^{th} receiver output to:

(1) Steer the beam in a particular direction,

(2) Correct for wavefront curvature (near-field focusing), and

(3) Correct for array out-of-planeness, if necessary.

Fig. 3-5 is a block diagram for a generalization of DIMUS beamforming in which weights W_k are applied to each receiver output to modify the beam pattern.

3.2.2 DIMUS/Adaptive Null -- This algorithm allows nulling of a coherent off-axis interference which arrives coincidentally with an on-axis signal, using hard-clipped data. The interference is nulled by subtracting from the k^{th} receiver output a coherent estimate of the interference obtained from the (k+1)st receiver output. The beam output is given by

$$b(n) = \sum_k \left[\epsilon_k (n-m_k) - W_{pk} \epsilon_{k+1} (n-m_k-\mu_{pk}) \right]; \quad pN_o \leq n \leq (p+1) N_o - 1$$

where

$$\epsilon_k(n) = \text{sgn}\,[s_k(n)].$$

The integer μ_{pk} is the sample delay corresponding to the propagation time of the interference between adjacent receiver locations. The optimum value of μ_{pk} is chosen by maximizing

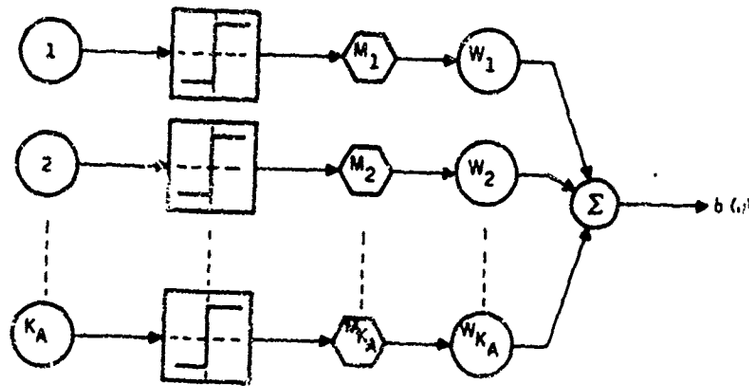

Figure 3-5. DIMUS Beamformer

$$\zeta_{pk} = \max_{i} \left[\sum_{n=pN_o}^{(p+1)N_o-1} \epsilon_i (n-m_k)\, \epsilon_{k+1} (n-m_k-i) \right]$$

on the p^{th} sample interval of length N_o, scanned over a range of delays encompassing the maximum interelement propagation time for interferences.

The weights W_{pk} are given by

$$W_{pk} = \begin{cases} 0; & |\mu_{pk}| \leq \delta_{pk} \\ 1; & |\mu_{pk}| > \delta_{pk} \end{cases} .$$

The constraint $W_{pk} = 0$ if $|\mu_{pk}| \leq \delta_{pk}$ prevents nulling of a signal within the beam, provided δ_{pk} is chosen equivalent to a half beamwidth in interelement sample delay.

Figure 3-6 is a block diagram of the DIMUS/Adaptive Null beamformer.

3.2.3 Cross-Correlation (Time-Averaged Product) of Beams - Denoting the two crossed arrays by their axis designation (x,y), if $b_i(n)$ is the beamformed output of the i^{th} array, the cross correlation of two beams, which provides a narrower beam than either of the individual beams, is given by

$$C(n) = \frac{1}{2L+1} \sum_{\ell=-L}^{L} b_x (n+\ell)\, b_y (n+\ell).$$

The correlation window, (2L+1) samples, is chosen equivalent to a pulse length.

This process is shown schematically in Figure 3-4b.

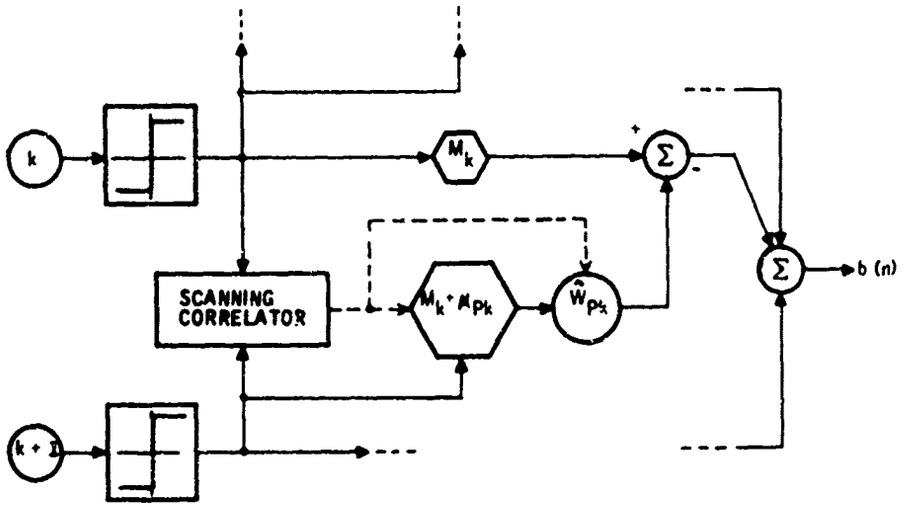

Figure 3-6. DIMUS/AN Beamformer

3.3 Three-Dimensional (3-D) Seismic Method

Three-dimensional treatment of seismic data is essential for underground applications. In the beamforming methods described above, this is accomplished by calculating the steering delays, m_k, to correspond to spherical angle pairs (θ, ϕ) in the directions of interest. After applying the appropriate delays to all receiver outputs and summing, coherent arrivals will add with similar polarities (i.e., in phase). The spatial phase coherence of reflected waveforms may be at least partially destroyed (i.e., wavefront distorted), by one of several causes, including:

- Rock inhomogeneity
- Nonplanar reflecting surface
- Nonplanar array locations
- Faulting

As a result, the beamformer output will be reduced, decreasing the likelihood that the reflection will be detected.

The three-dimensional seismic method is an alternative approach which is expected to be more robust for the conditions listed above. The 3-D method will be easier to implement, but will place a greater interpretation burden on the operator.

The 3-D method can best be described with reference to a single source at the center of a large square array of receivers. The outputs of the receivers, in response to a transient input from the source, are recorded and displayed simultaneously on a square grid. The grid corresponds to the locations of the individual receivers. For a reflecting surface parallel

to the plane of the array, the reflection will be observed as a circular pattern centered on the source location. The circles expand from the fixed center with increasing time. If the reflector is dipping, then the center of the pattern is shifted updip to a point which is the projection of the image of the source onto the plane of the array (Fig. 3-7).

The recorded signals from the receivers are viewed on a screen as a variable intensity display of all the receiver outputs at a particular time. As time is varied by scanning through the record, reflections (and other coherent events) will appear as circular rings or arcs of circles, move across the screen and then disappear.

The display constantly changes as time is increased and deeper and deeper reflections appear. The rings of reflected energy get thinner and move more slowly as they expand toward the edges of the display. Since the rings of reflected P-wave energy will move at a different rate than those of S-waves, and both will move at different rates than noise, they are distinguishable.

When crossed arrays are used to simplify field procedures, the interpretation becomes somewhat more complex. For a single source, all rays spread out radially from the source to the N^2 receivers. For a crossed array of N sources and N receivers, N^2 signals are still recorded, but the circular symmetry of the single source geometry is lost. As a result, the circular patterns are distorted into ellipses, whose eccentricities depend on the angles of dip of the reflectors.

Figures 3-8 and 3-9 are simulated displays for reflectors dipping to the left (Fig. 3-8) and to the lower left (Fig. 3-9). Individual frames, from left to right, represent successive instants of time at ten microsecond increments, with an assumed P-wave velocity of 17,500 ft/sec. The purpose of the simulation was to get a preliminary evaluation of the

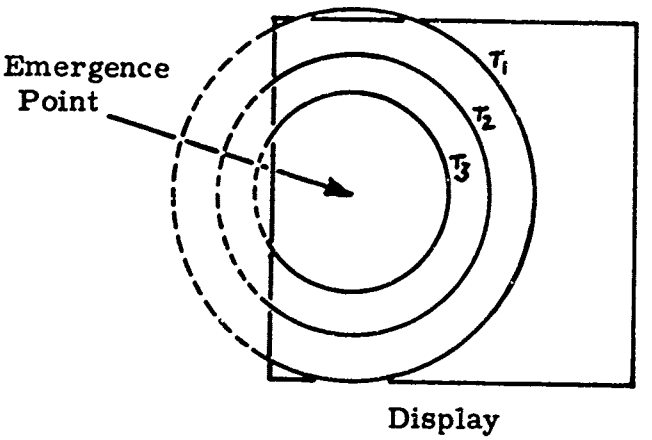

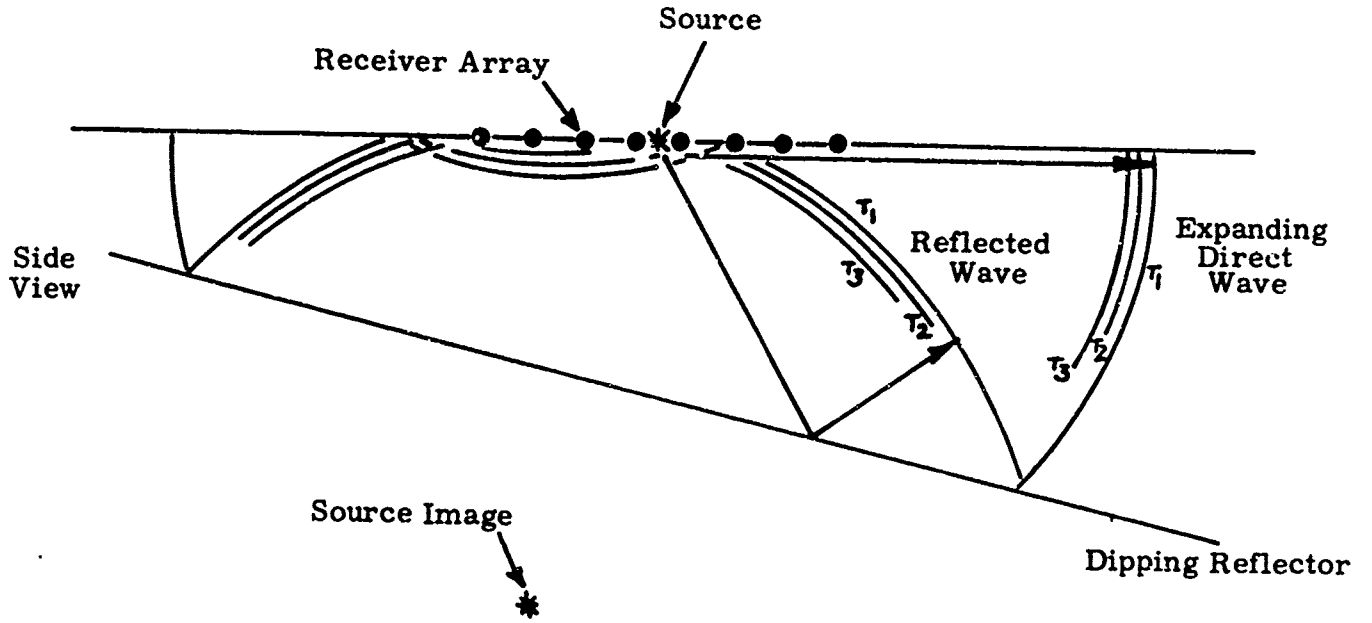

Figure 3-7. 3-D Method

Figure 3-8. Simulated Displays for Reflectors Dipping to the Left

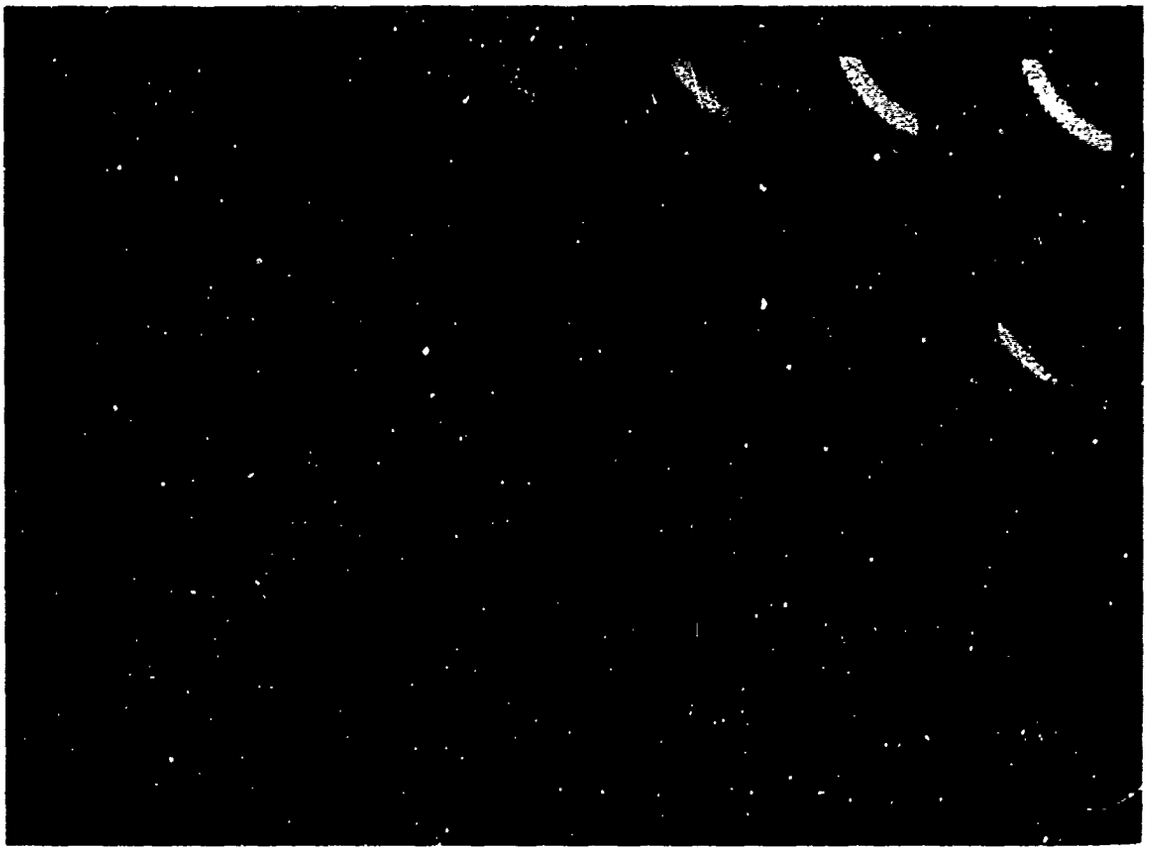

Figure 3-9. Simulated Displays for Reflectors Dipping to the Lower Left

applicability of the 3-D method to relatively small arrays, which might be practical for underground use. Figures 3-8 and 3-9 simulate 21 x 21 element arrays, in contrast to 48 x 48 element arrays used for seismic exploration by the 3-D method. The seismic pulse was assumed to be a damped sinusoid. The element spacing is one-half wavelength at the dominant frequency of the pulse. Consequently, the simulated array aperture is ten wavelengths square. Sixteen intensity grey levels were used.

Wavefront distortion from causes listed above, which may be expected to severely degrade beamforming techniques will merely distort the patterns observed with the 3-D method. To the extent that the patterns are still recognizable, the reflections may be more detectable than they would be with the beamforming technique. Also, faults on a reflection will break its circular pattern, and the location of the break indicates where the fault is. Again, using beamforming, the presence of a fault will partly destroy the phase coherence of the reflected wavefront, and reduce the output of the beamformer accordingly. This represents an advantage of the 3-D method for underground applications, since fault detection is of high priority.

SECTION IV

4.0 SEISMIC PROTOTYPE SYSTEM DEVELOPMENT

The objective for the first six months' phase of the present program has been the design and construction of a seismic system for further field experiments to evaluate beamforming and 3-D seismic array methods. The goal is a prototype system for application of the 3-D method which can also provide recordings for subsequent "playback", digitization, and digital processing in the laboratory for evaluation of beamforming. Desirable characteristics of the system include:

(1) Portability

(2) Low cost

(3) Minimum power requirements

(4) Flexibility

(5) Simplicity

(6) Maximum accuracy and speed of operation

4.1 System Concept

A functional block diagram of the system is shown in Figure 4-1. A seismic recording system consisting of single source transmitter, single receiver and optical recorder produces variable density film transparencies which can be viewed in the field using the display system, or digitized in the laboratory.

The display system contains a coherent fiber optics image converter. The film format consists of a variable density record from each array element side-by-side along one axis, with record time along the other axis (elapsed

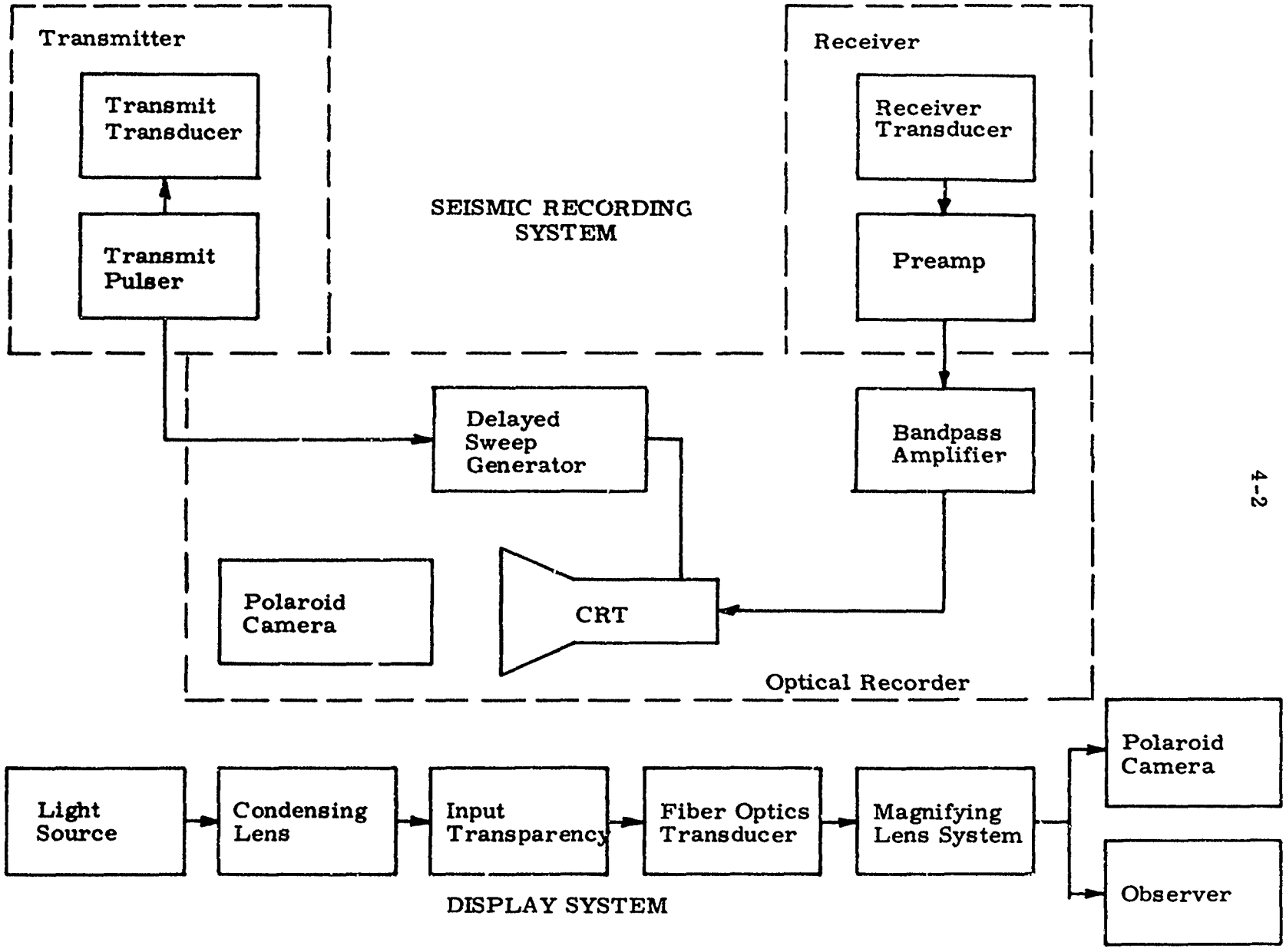

Figure 4-1. Prototype Seismic/Acoustic System

time relative to transmit pulse). The fiber optics converter has a row of fiber bundles which samples all array element records corresponding to a particular time. The fiber bundles are rearranged at the other end of the device into a square matrix corresponding to the seismic array. The image observed at the square end is the array output at a particular time as required. Time is scanned by moving the transparency.

A single record can be displayed at a time on the cathode-ray tube (CRT). The Z-axis (intensity) of the CRT is modulated by the receiver response to a transmitted pulse. A linear sweep signal deflects the CRT spot to produce an intensity-modulated line display of the received signal versus time. The line is photographed, producing a variable density record of one element of the array. The receiver is moved to the next array location, the film is moved one record width, and the process repeated. This procedure is repeated until all array locations have been recorded.

Time synchronization is maintained between records by triggering the sweep generator by the pulsed source transmitter. Delaying the triggered sweep allows a selected time interval to be recorded.

The delayed sweep generator function was implemented in the system by a Biomation Model 802 Transient Recorder. This commercial unit provides a memory function, which allows nonrepetitive seismic sources, such as hammers and other impact devices, to be used for more flexibility.

Polaroid Type 55P/N film was specified for use in the recording camera, as a matter of convenience for field use. The film provides both a transparency and a print, has sufficiently fine grain in the negative for the required magnification, and good grey scale range.

Figure 4-2 shows the completed seismic recording system, less camera. The configuration shown includes a borehole receiver and spark transmitter, which was developed as a borehole source. The control unit on the right also has provision for a piezoelectric ceramic (PZT) transducer (not shown) which will be evaluated as a surface source.

Descriptions of construction details and modifications are given in the discussion to follow for the optical recorder, receiver, and display subsystem. The seismic source development will be discussed in Section 5.0.

4.2 Optical Recorder

The optical recorder consists of the Biomation Model 802 Transient Recorder, Tektronix Type 602 Display Unit, and modified Tektronix C-27 Oscilloscope Camera (Fig. 4-3).

The 802 digitally stores 1024 samples of the signal from the receiver accelerometer (also shown). The samples represent the receiver output over a time interval determined by the sweep time and delay settings chosen. Thus, for example, it is possible to gate out the first millisecond of receiver output and record the succeeding 5 milliseconds.

The contents of the digital memory are converted to a repetitive analog output signal synchronized with a repetitive two-millisecond linear sweep. The Y-output (signal) and X-output (sweep) drive the Z-axis (intensity) and Y-axis (vertical deflection), respectively, of the 602 CRT display. The receiver output is thus made repetitive and displayed as an intensity-modulated line, just visible in the center of the CRT face in Figure 4-3. Figure 4-4 shows a close-up of the CRT face.

Figure 4-2. Seismic Recording System (Camera Not Shown)

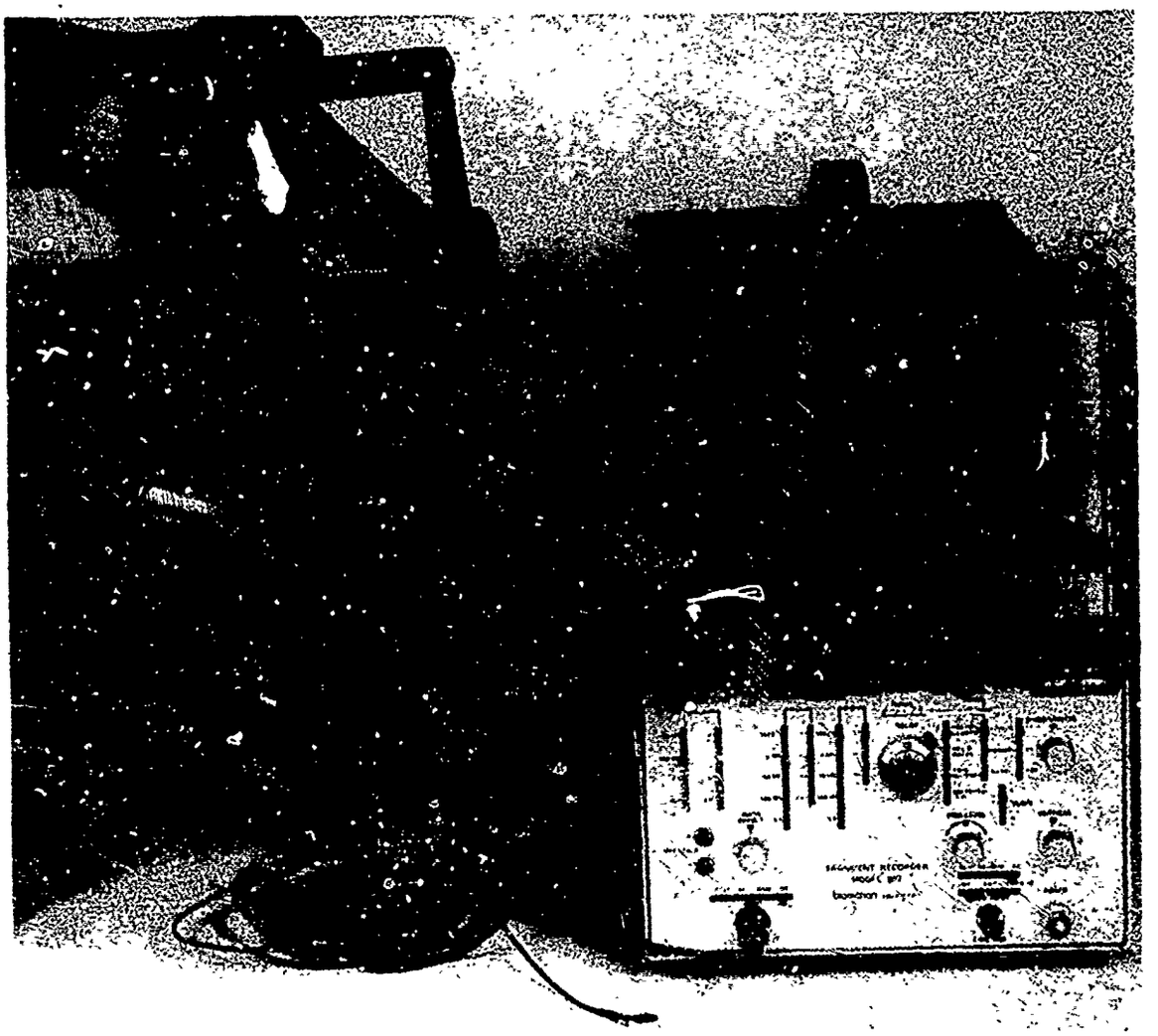

Figure 4-3. Variable Intensity Photographic Recorder

Figure 4-4. Close-Up of CRT Face, Showing Intensity-Modulated Trace

A vertical slit aperture, 16 mils wide, has been added to the CRT faceplate. The slit serves to provide a uniform record width. The CRT spot size normally increases with intensity, which is proportional to the receiver output voltage. To avoid variations in trace width with signal amplitude, the slit was provided, together with a circuit to provide a high frequency triangular wave signal drive on the CRT X-axis (Fig. 4-5). This high frequency "dither" produces a broadened trace of uniform intensity, many times the width of the slit. In addition to providing a uniform record width, this approach eliminates horizontal drift as a possible source of error.

The CRT has only an outline graticule, so that no lines will appear in the film record. (An external time-mark generator can be used, however, to record variable-density time lines, when desired.) The outline graticule appears as a fine line near the top and bottom of the slit which can be used as index marks for initial vertical trace positioning and periodic correction of vertical drift with the CRT vertical position control, if necessary. The phase coherence of array outputs can thus be maintained to a high degree of accuracy.

4.2.1 Camera Modifications -- The camera assembly consists of camera, camera back and film holder, and film advance mechanism. The addition of the lead screw detented film advance was the principal modification, although changes were also made to the camera back.

The recording film must be precisely movable in increments slightly less than one trace width in order to avoid undesirable gaps between successive traces on the film. This was accomplished with a lead screw to move the camera back. The lead screw contains 32 threads per inch and is detented at quarter-turns (Fig. 4-6), so each detent position represents a film motion of 1/128 inches or about 0.0078". The camera magnification is 1:0.5, so

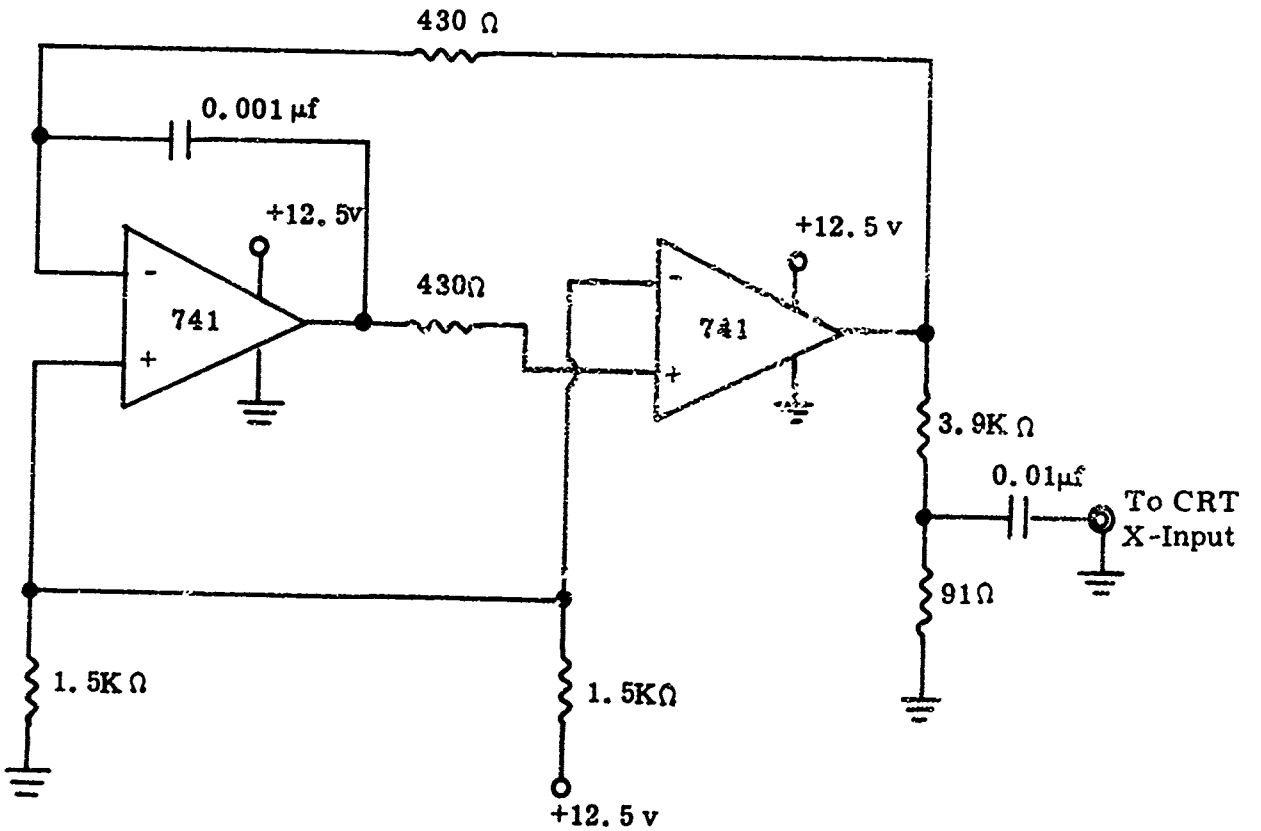

Figure 4-5. Triangle Wave Generator

Figure 4-6. Film Motion Mechanism

that the image of the CRT slit aperture is half the width of the slit. A slit width of 0.016 inch produces a 0.0080-inch record, which allows 0.0002 inch record overlap.

The modified camera will record 128 records per inch of film, without gaps or excessive overlap between adjacent records. Figure 4-7 is a test recording, containing 384 traces. The recorded signal was a sine wave, with the frequency varied slightly between adjacent traces. Resolution along the time axis appears to be at least 100 cycles/sweep. For a ten millisecond sweep, compatible with penetration up to about 100 feet, this resolution provides a frequency response of about 10 KHz.

A standard 4x5 Graflok camera back was modified with extender plates to allow movement of the film over a total distance of four inches. The four-inch allowed movement permits the recording of up to 512 array outputs. Thus, maximum array dimensions are 22 x 22 = 484 elements. The lead screw was made long enough to accommodate the four-inch format.

4.2.2 System Sensitometric Measurements -- Densitometer measurements were made on the developed film to optimize the combination of:

(1) Signal input levels to the CRT Z-axis,

(2) Camera aperture, and

(3) Exposure time.

The best combination consisted of:

(1) Signal level: 0 - 1.0 volt

(2) Aperture: f/5.6

(3) Exposure time: 1 second

Figure 4-7. Optical Recording Test, Sine Wave Input, 500 Hz to 16,000 Hz, Twelve Traces per 500 Hz Frequency Increment, 10 Millisecond Sweep

A representative graph of film density versus input voltage is shown in Fig. 4-8. The range of density is such that 16 gray levels were easily distinguishable.

4.3 Borehole Receiver

The receiver was designed to be used either in a borehole or on the surface of the mine or tunnel opening. An accelerometer is used as the transducer. For surface mounting, the accelerometer can be cemented or used with a detachable stud.

A pneumatic method was devised for clamping the accelerometer to the side of a small diameter borehole. Semi-rigid plastic tubing is used to position the accelerometer in the hole and to inflate the rubber clamping hose, using a bicycle tire pump.

The assembly is pictured in Fig. 4-9, inflated inside a 1-1/2 inch diameter plastic tube. A replaceable steel or aluminum button is used to hold the accelerometer in place, provide good mechanical coupling to the rock surface, and protect the accelerometer. Insulated washers are used for electrical isolation.

Figure 4-10 shows a closeup of the device wit' the accelerometer removed. The rubber hose is clamped to a brass cylinder, which is hollow at one end for inflating the tube.

4.3.1 Accelerometer -- A commercially-available piezoelectric accelerometer, Endevco Model 2220C, was chosen as the transducer. Selection criteria included: 1) small size, 2) high resonant frequency, 3) center-hole configuration, and 4) sensitivity (Table IV-1).

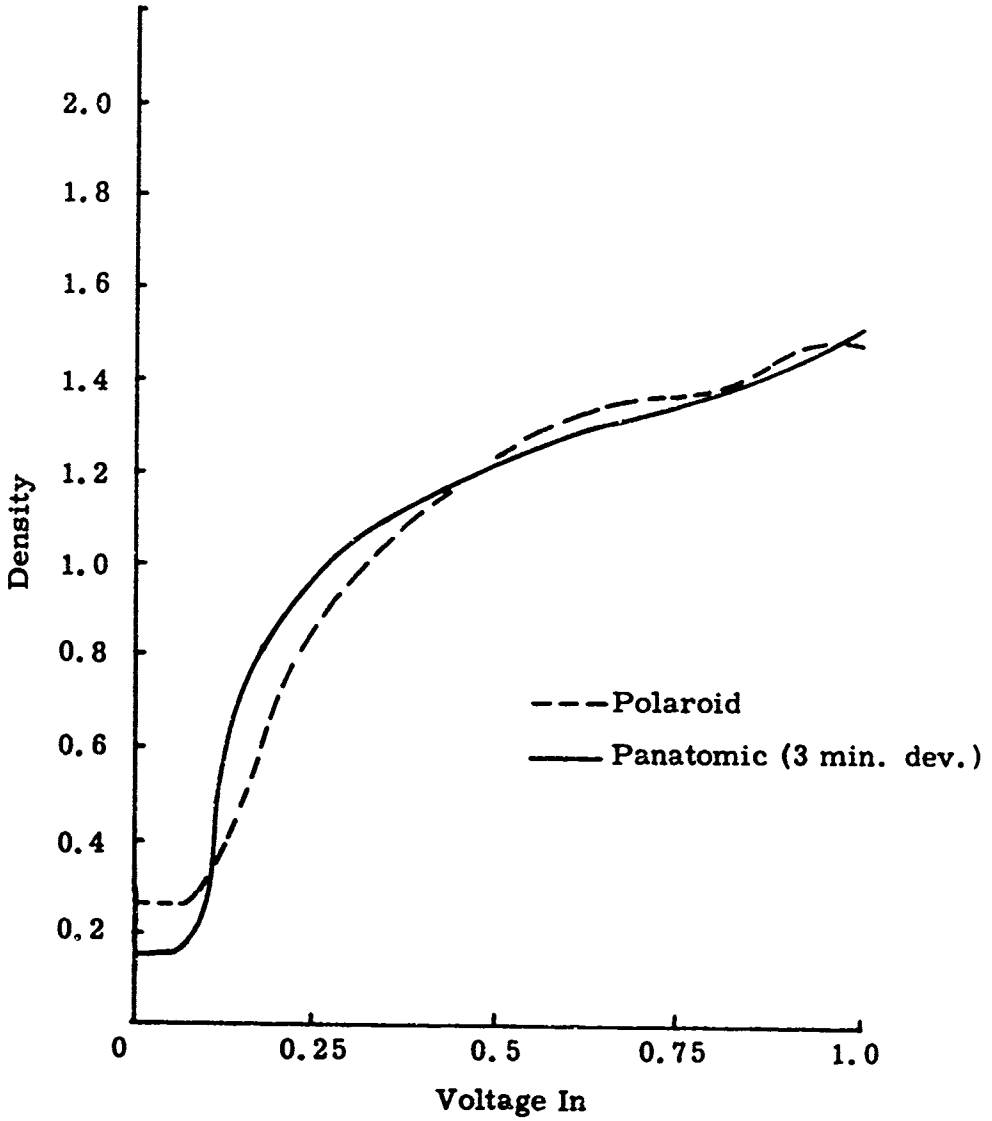

Figure 4-8. Gray Scale Measurements of Panatomic and Polaroid P/N Films

Figure 4-9. Borehole Receiver (Inflated)

Figure 4-10. Borehole Receiver (Partially Disassembled)

Table IV-1. Specifications for Model 2220C Accelerometer

Charge Sensitivity	2.8 pC/g, nominal
Voltage Sensitivity*	3.0 mV/g, nominal
Transducer Capacitance	750 pF, nominal
Mounted Resonant Frequency	50,000 Hz, nominal
Resistance	20,000 MΩ, minimum at +72° F 5000 MΩ, minimum at +350° F
Frequency Response	2 Hz to 10,000 Hz
Transverse Sensitivity	5% maximum, 2% special selection
Amplitude Linearity	Sensitivity increases approximately 1% per 500g, 0 to 5000g

*with 200 pF external capacitance

The high frequency response of a piezoelectric accelerometer is determined by its mechanical resonance. It can be represented as an undamped resonant spring-mass system, and provides a flat response to acceleration inputs up to about one-fifth its resonant frequency, with minimum phase shift. For pulse measurements, accelerometer overshoot and ringing are minimized if the natural period is less than one-fifth the pulse duration, or less than about one-third the pulse rise time. Since we are concerned with pulse durations of about 100 microseconds, and frequencies below 10 KHz, the 50 KHz resonant frequency of the 2220C accelerometer was considered adequate.

The low frequency response of a piezoelectric accelerometer is determined when used with voltage amplification by the RC time constant of the total capacitance (transducer, cable and input capacitance of the amplifier) along with the input resistance of the amplifier. When charge amplification is used, the low frequency response is determined primarily by the amplifier response.

4.3.2 Amplifier -- A bandpass amplifier was incorporated into the receiver, whose primary purpose is to provide high frequency roll-off, so that accelerometer resonance response is reduced, and to provide a low frequency response which will be independent of cable capacitance, and therefore the length of cable used. The charge amplifier circuit, with low and high frequency cutoff points at 2 KHz and 8 KHz and 6 db/octave rolloff, is shown schematically in Fig. 4-11.

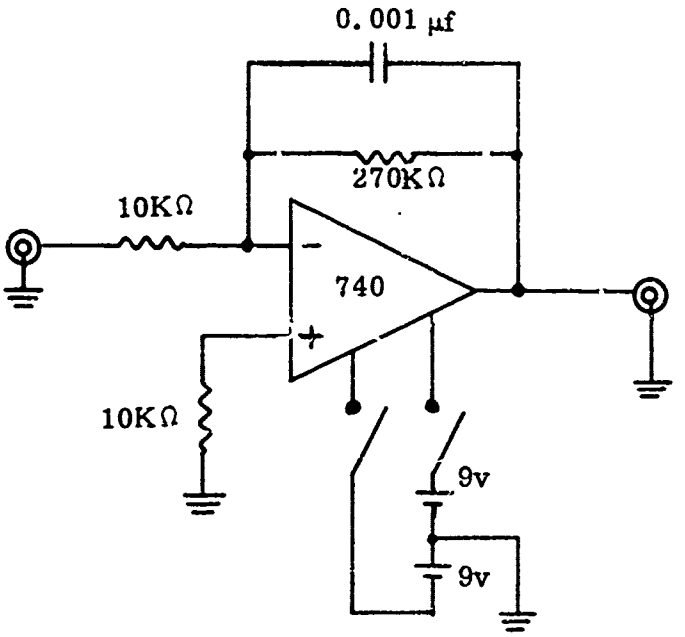

Figure 4-11. Accelerometer Bandpass Amplifier

SECTION V

5.0 SEISMIC SOURCE EVALUATION AND DEVELOPMENT

A substantial effort has been directed in this phase toward the evaluation of possible seismic sources for use on the rock surface, as well as in a borehole. A series of measurements were taken by the University of Minnesota under subcontract for a variety of surface sources, primarily of impact type. A summary of these measurements is contained below. In addition, a pulsed piezoelectric source, developed by the U.S. Army for tunnel detection and recently tested as a seismic source in a coal mine, was acquired for evaluation as source transmitter in planned underground data acquisition. Finally, an underwater spark transmitter was developed to serve as a downhole source for array experiments.

5.1 Summary of Impact Source Measurements

A series of measurements was taken to obtain characteristics of seismic waveforms produced by a variety of impact-type sources including:

(1) A hammer, directly onto the rock surface,

(2) Hammer, onto pins embedded in the rock,

(3) Hammer, onto rods in contact with the rock, both on the surface and at the bottom of a hole, and

(4) Explosive- and gas-driven projectiles.

Waveforms were detected by piezoelectric accelerometers and converted to permanent stripchart records (with special instrumentation to provide frequency response to 100 KHz) and oscilloscope photographs. The waveform was passed through a filter which permitted variable bandpass filtering. The accelerometer and source placements were selected to yield results for:

a) Transmission through a concrete block,

b) Propagation along the surface,

c) Detection within a drill hole.

Accelerometer tests within the drill hole were carried out using two methods of holding the accelerometer against the side of the hole: mechanical and pneumatic. The results indicated no difference in rise time, amplitude, or total waveform.

Frequency content of the waveforms did not change drastically among the various impact-type sources. Most of the energy is in the range 5-20 KHz, with substantial contributions up to 30-40 KHz and negligible energy below 2 KHz. Impacts onto rods, and particularly impacts onto embedded pins, do give somewhat more high-frequency components than direct impact onto the rock.

The repeatability of these waveforms is reasonably good for frequencies of less than 15-20 KHz, but poor for higher frequencies.

One measure of the frequency characteristics of the source waveforms is the rise time (zero to peak) of the direct P wave. This measure has the advantage that it will be unaffected by reflections and other disturbances. It was found that:

(1) Hammer impact directly onto the concrete surface gives a rise time of the order of 30-40 microseconds.

(2) Impact onto an embedded pin reduces the rise time to 10-15 microseconds.

(3) Impacts onto a small center punch and a nailset gives rise times of about 25 and 15 microseconds, respectively.

(4) Impacts onto a star drill and a large center punch gives rise times of about 35 and 30 microseconds, respectively.

(5) Impacts onto the steel and aluminum rods gives rise times of about 20 and 15 microseconds, respectively.

The explosive stud driver with projectile yields two distinct arrivals. Arrival time for the second varies with explosive charge size but falls in the range 350-500 microseconds. Amplitudes are 5-10 times as great as for the first arrival. A consideration of possible explanations leads to the conclusion that the smaller first arrival is from the explosive gases and the second from the projectile impact.

It was concluded that impact sources have the following advantages as possible seismic sources for the excavation seismology program:

(1) They are rapid, cheap, light, flexible.

(2) They bypass problems associated with rough or fractured rock surfaces.

(3) They are rich in frequencies at the range of interest for this program, say 5-20 KHz.

(4) Rise times are quite satisfactory, especially for impacts onto rods or embedded pins.

(5) Energy output is good.

(6) Waveform repeatability is adequate in the frequency range of interest, although poor at higher frequencies (which could be filtered out if desired).

(7) Source location can be precisely defined for array studies, especially for impacts onto rods or embedded pins.

5.2 Underwater Spark Source Development

Requirements for a high energy seismic impulse source, which could be used at depths up to 15-20 feet in a small diameter borehole, led to the development of an underwater spark source. The source was required to be repetitive, portable, and have a pulse duration of not more than about 100 microseconds, with substantial energy output at frequencies below 10 KHz.

Other possibilities which were considered, but appeared less advantageous than an underwater spark included:

(1) Detonators (blasting caps),

(2) Air gun,

(3) Piezoelectric or magnetostrictive transducer,

(4) Propane/air exploder, and

(5) Electromechanical or mechanical impactor.

Blasting caps, although fairly inexpensive and convenient, would release gaseous explosion products into the water-filled hole. Since we would want to fire repeatedly several hundred times in the same hole, the pulse characteristics likely would change. Also, firing time delay uncertainties would adversely affect array output time alignment.

Air guns, which have been used as sources for offshore seismic exploration, operate on the sudden release of a small volume of high pressure air. The output pulse of existing air guns was too long in duration and low in frequency for the underground seismic problem, and it did not appear feasible to change it substantially. Again, time synchronization would also be a problem.

Piezoelectric or magnetostrictive transducers have excellent repeatability and can be precisely triggered. However, size was considered to be a problem. The pulse energy produced is directly related to the size of the device. For a small diameter hole, the allowable size would not produce sufficient energy output.

A propane/air exploder was a promising alternative. A very high output energy pulse of short duration could be achieved, and the hole would not need to be filled with water for coupling the seismic pulse to the rock. A preliminary design of such a device was obtained; however, the propane source would have to be retrieved from the hole after each shot for reloading and replacement of a frangible disc. Since this operation would be undesirable, no further development of this source was attempted.

Mechanical impactor concepts were severely limited by the limited hole size, and again, time synchronization would be a problem with mechanical devices.

5.2.1 The Electrohydraulic Effect -- An underwater spark produces a pressure pulse which has found application as a sonic source (Ref. 1) and has been investigated for rock fracturing and comminution (Ref. 4). The underwater spark is produced by the sudden discharge of capacitively stored electric energy across a submerged electrode gap. Initiation of the spark creates a plasma and vapor channel between the two electrodes. Extremely high pressures are produced within the channel, which are transmitted to the surrounding water. The channel then expands as a bubble, compressing the water until the vapor pressure in the bubble falls below the hydrostatic pressure. The pressure pulse transmitted to the water is similar to that from an explosion, rising rapidly and decaying more slowly.

5.2.2 Bubble Pulsations -- The water in the immediate region of the expanding bubble has a large outward velocity and the diameter of the bubble increases rapidly. As the pressure falls below the equilibrium level, the motion is reversed abruptly, and the bubble contracts.

As the bubble expands and contracts, a pressure wave propagates radially outward. From incompressible fluid theory, it is known that pressure depends on the square of the rate of bubble expansion and contraction. This rate is greatest when the bubble is at the point of minimum volume. Thus, pressures are significant only near the point of maximum contraction. The peak pressure in the bubble pulse is no more than ten to twenty percent of that in the main shock wave but the duration is much greater (Ref. 2). Usually, only the first bubble pulse is of practical importance.

5.2.3 Circuit Analysis -- Figure 5-1 contains a functional block diagram of the spark source. The source is basically a series network of a charged capacitor, fast discharge switch, connecting wires, and the electrode gap. Figure 5-2 is the equivalent electrical circuit where:

V_o = Voltage across charged capacitor

C_c = Capacitance of storage capacitor

L_c = Inductance of storage capacitor

L_s = Inductance of switch capacitor

R_s = Resistance of switch capacitor

C_ℓ = Capacitance of cable capacitor

L_ℓ = Inductance of cable capacitor

C_g = Capacitance of electrode gap

L_g = Inductance of electrode gap

R_g = Resistance of electrode gap

The shunt capacitances associated with the cable and electrode gap are negligible, resulting in the simplified circuit of Fig. 5-3. Here:

L = Total inductance = $L_c + L_s + L_\ell$

R = Total resistance, not including gap = $R_s + R_\ell$

For a sudden closure of the switch, the equation describing the discharge current is:

$$L \frac{dI}{dt} + RI + \frac{1}{C} \int I \, dt = 0,$$

whose solution (underdamped case) for $I (t = 0) = 0$ is

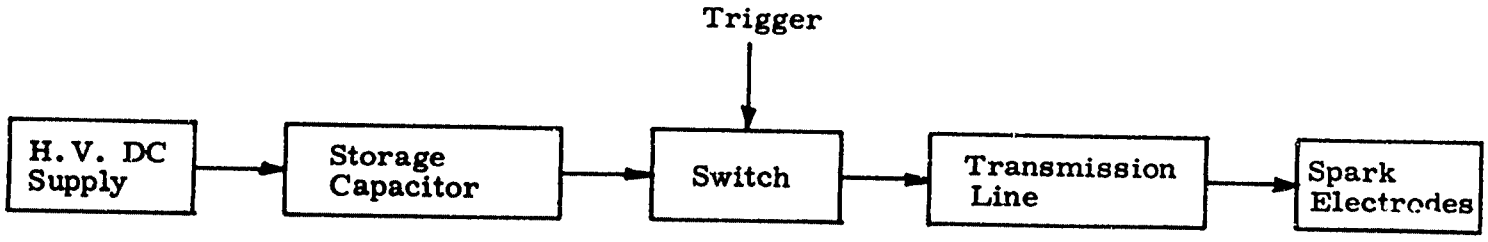

Figure 5-1. Spark Source Block Diagram

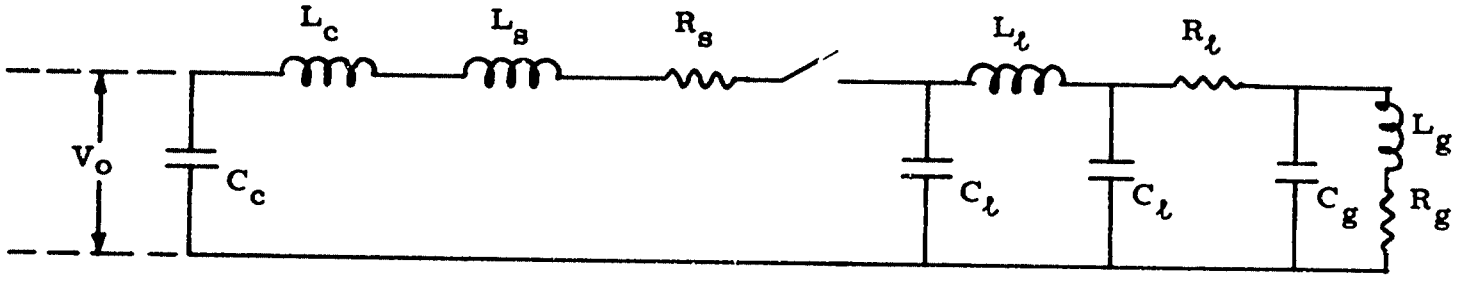

Figure 5-2. Spark Source Equivalent Circuit

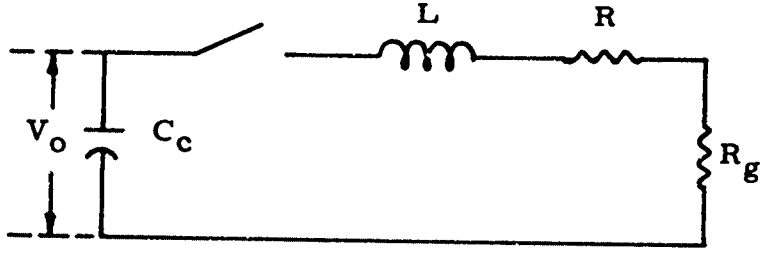

Figure 5-3. Simplfied Circuit

$$I(t) = \frac{V_o}{\omega_o L} e^{-bt} \sin \omega_o t$$

where

$$\omega_o = \sqrt{\frac{1}{LC} - \frac{R^2}{4L^2}} = \text{frequency of damped sinusoid}$$

$$b = \frac{R}{2L} = \text{damping factor.}$$

The maximum value of current is determined from the condition

$$\left.\frac{dI}{dt}\right|_{I = I_{max}} = 0.$$

Thus,

$$I_{max} = \frac{V_o}{\omega_o L} e^{-bt_{max}} \sin \omega_o t_{max}$$

$$t_{max} = \frac{1}{\omega_o} \tan^{-1} \left(\frac{\omega_o}{b}\right) = \text{time of peak current.}$$

5.2.4 Energy Considerations -- The total energy stored in the capacitor is equal to $E_{total} = \frac{1}{2} CV_o^2$. The energy dissipated by the spark is given by

$$E_{spark} = \frac{R_g}{R + R_g} E_{total}.$$

Maximum efficiency requires that $R << R_g$. The spark resistance R_g is determined by the maximum electrode gap which will produce breakdown at the voltage V_o.

5.2.5 Electrode Design -- The coaxial electrode design which evolved during the spark source development is shown in Fig. 5-4. The high voltage electrode is the center screw. The electrode exposed area is minimized to eliminate leakage paths as much as possible. The electrode gap is filled with a polyester-glass washer to provide mechanical rigidity and eliminate fouling. Sparking thus occurs around the periphery of the electrode gap.

The maximum gap size for voltages up to 2.5 Kv in tap water is about 0.025 inch. We found that rubber "O" rings, placed over the gap and held in place by the linen bakelite cap, would effectively suppress the formation of a bubble pulse. Figure 5-5 shows the electrode housing, partially disassembled. The electrode structure can be simply unscrewed for replacement.

This design was found to be highly rugged and to provide reliable, repeatable sparking.

5.2.6 Experimental Results -- The resistance and inductance of the spark circuit can be estimated from a graph of the discharge current versus time:

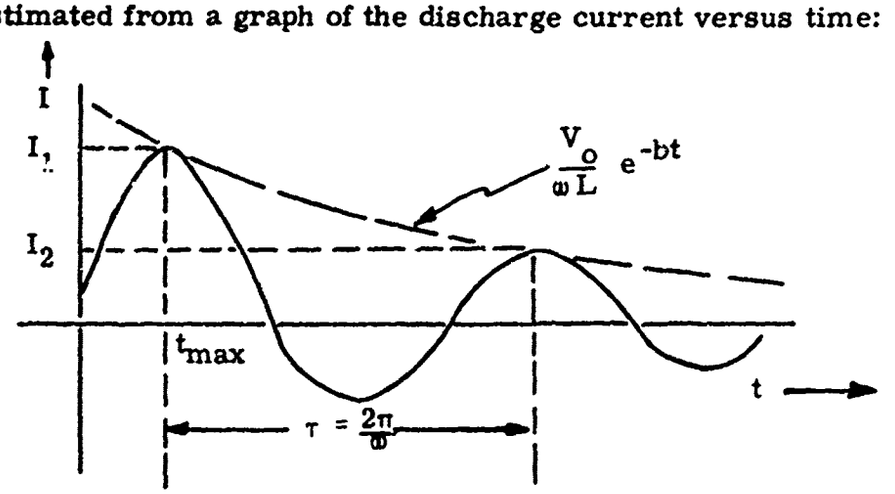

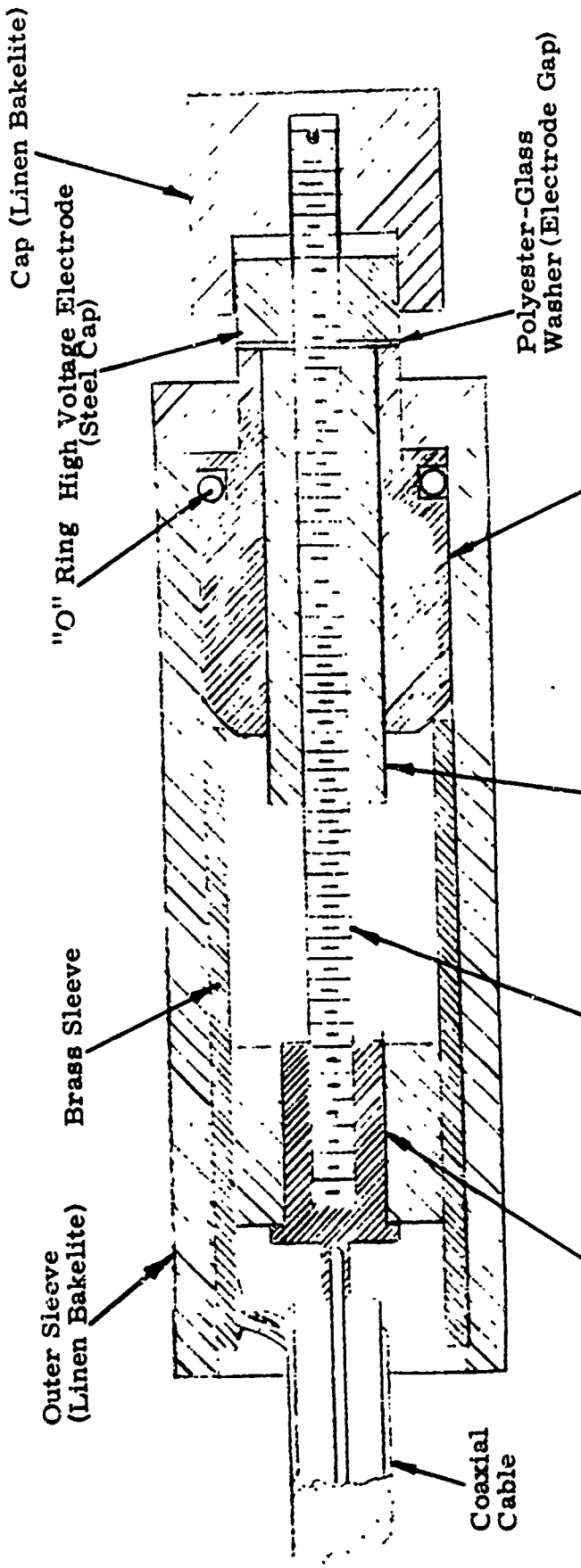

Figure 5-4. Spark Source Electrode Design

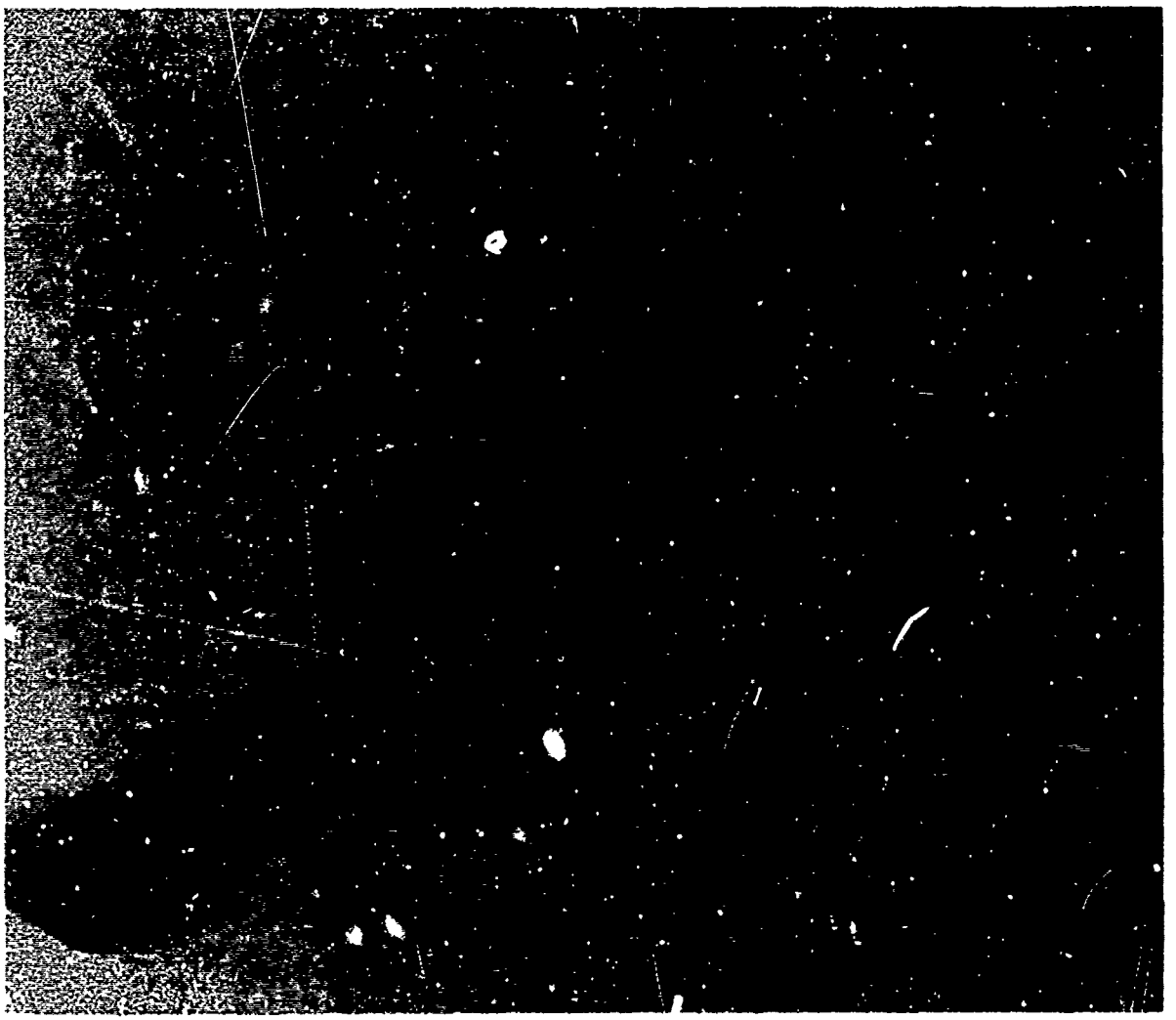

Figure 5-5. Electrode Housing, Partially Disassembled

The frequency is estimated from the time difference τ between successive current peaks. The damping factor is determined from the ratio of current values:

$$\delta = \ell n \frac{I_1}{I_2} = \ell n \frac{e^{-bt\ max}}{e^{-b\ (t_{max} + \tau)}}$$

$$= b\tau$$

or,

$$b = \frac{\delta}{\tau} = \frac{R}{2L}$$

Also,

$$\frac{1}{LC} = \omega_o^2 + b^2 = \frac{4\pi^2}{\tau^2} + b^2$$

Figure 5-6 is the current waveform with (a) the electrode gap shorted, to measure circuit resistance, and (b) during sparking with the electrode gap immersed in tap water. The value of τ, from Figure 5-6 (a) is approximately 30 microseconds. Calculated values of circuit inductance and resistances, with shorted gap and during sparking are summarized in Table V-1.

The experimental results indicate that approximately half of the total resistance is due to the gap; therefore, half the energy is dissipated in the spark. Of this, perhaps half is radiated as acoustic energy in the shock wave. The total energy for C = 15 microfarads, V_o = 2.5 kilovolts is about 48 joules. The estimated useful seismic energy per pulse, therefore, is 12 joules (1 joule = 1 watt-second).

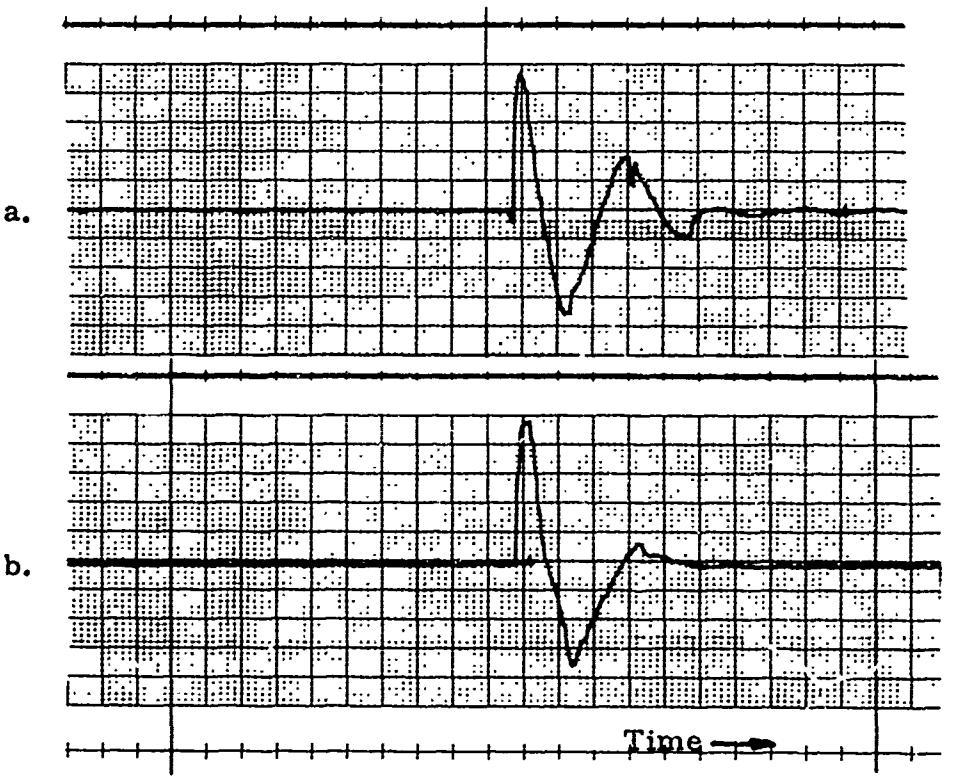

Figure 5-6. Current Waveforms for:
(a) electrode gap shorted
(b) during sparking
(One division = 2 microseconds)

5.2.7 Energy Spectrum of Pressure Pulse -- The pressure pulse from an underwater spark is approximately a decaying exponential:

$$P = P_o e^{-mt}$$

where the decay constant m is approximately the same as the discharge circuit time constant, to within 10% (Ref. 1).

The acoustic energy contained in the pressure pulse is

$$E_p = \frac{1}{\rho c}\int_o^\infty |\, p\,(t)|^2\, dt$$

where ρc is the acoustic impedance of wate e corresponding frequency spectrum is given by the Fourier Theorem a

$$E'_p(f) = \frac{2P_o^2}{\rho c}\left[\frac{1}{m^2 + (2\pi f)^2}\right]$$

The output energy for the spark source is seen to decrease with frequency. At f = 10 kHz, assuming $m \cong b = b \times 10^4\ sec^{-1}$, the output spectrum is down by a factor of twc.

5.2.8 Spark Source Circuitry -- Figure 5-7 is a schematic diagram of the high voltage supply, storage capacitor and switch. Triggering of the pulse can be done either manually by pushbutton, or remotely. An autotransformer and meter have been incorporated to allow the discharge voltage, V_o, to be continuously adjustable. A synchronizing pulse is also provided to trigger the Biomation recorder. The circuit is enclosed in a portable case, together with triggering circuitry for a piezoelectric transducer, which will be described in Section 5.3. The case and front panel are shown in Figure 4-2. In Figure 5-8, the panel has been removed.

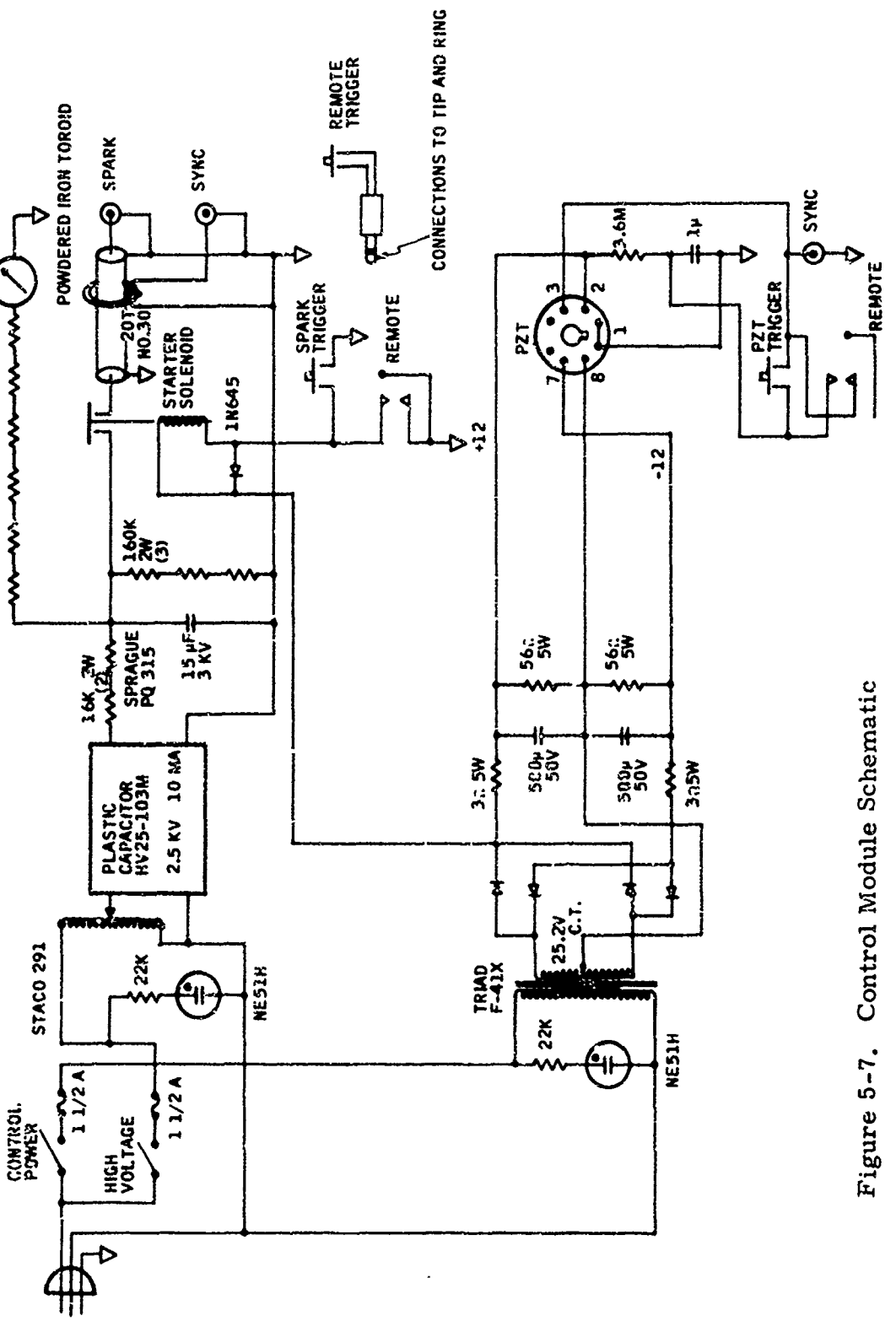

Figure 5-7. Control Module Schematic

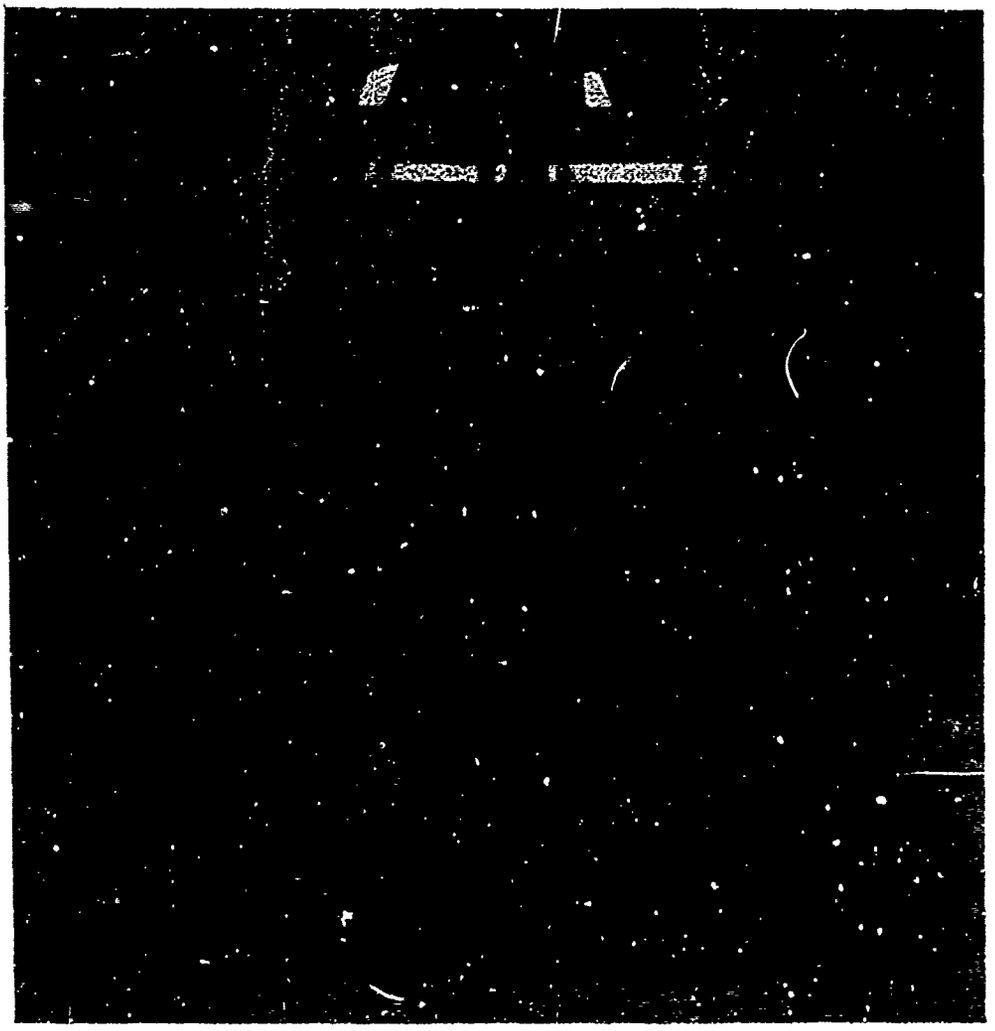

Figure 5-8. Control Module with Front Panel Lowered

The discharge circuit includes about 15 feet of RG 8/U cable, connecting the spark gap with the charging circuit. The total resistance of the discharge circuit, including the cable, was derived in Section 5.2.6 as 0.09 ohms. The charging time is approximately five seconds.

Table V-1. Measured Circuit Parameters

	Gap Shorted	Underwater Spark
τ, sec	30×10^{-6}	30×10^{-6}
$\frac{I_1}{I_2}$	2.5	6.0
δ	0.9	1 3
b, sec^{-1}	3.0×10^{4}	6.0×10^{4}
L, microhenries	1.5	1.5
Resistance, ohms	R = 0.09	R + Rg = 0.18

5.3 Piezoelectric Transducer

A piezoelectric transducer, similar to one developed by the U.S. Army for seismic tunnel detection (Ref. 6) and previously tested by the U.S. Bureau of Mines in underground coal mines, is an attractive possibility as a seismic surface source in hard rocks.

The transducer, pictured in Figure 5-9, is based upon the rapid discharge of an electrical charge stored in the capacitive ceramic elements of the transducer. The transducer is charged slowly from a high voltage source, and the impulsive discharge provides a high-peak-power mechanical output pulse.

The capacitance of the transducer is 0.30 microfarads and the operating voltage is 3 kilovolts for a discharge energy per pulse of 1.35 joules. A series inductance of 6 millihenries is included to provide a pulse rise time of 47.5 microseconds, and a series resistor provides optimum damping.

Figure 5-9. Piezoelectric Transducer

For this program, we provided a triggering circuit and DC power supply to operate the piezoelectric transducer. The circuit schematics were included in Figure 5-7. The electronics are housed with the spark source electronics, so that either source may be used interchangeably.

SECTION VI
REFERENCES

1. Caulfield, D.D. Predicting Sonic Pulse Shapes of Underwater Spark Discharges. Woods Hole Oceanographic Institutions, Woods Hole, Mass., March 1962, 16 pp.; ASTIA AD 276553.

2. Cole, R. H. Underwater Explosions. Dover Publications, New York. 1965.

3. Dunkin, J. W. and F. K. Levin. Isochrons for a Three-dimensional Seismic System. Geophysics, v. 36, No. 6, 1971, pp. 1099-1137.

4. Kutter, H. K. The Electrohydraulic Effect; Potential Application in Rock Fragmentation. Bu Mines Rept. of Inv. 7317, 1969, 35 pp.

5. Milder, D.M. and W.H. Wells. Acoustic Holography with Crossed Linear Arrays. IBM J. Res. Dev., Sept. 1970, pp. 492-500.

6. Owen, T.E. et al. An Improved Experimental Seismic Tunnel Detector. Interim Tech. Rept., Contract No. DAAK02-68-C-0033, Southwest Research Institute, San Antonio, Tex., March 1969, 62 pp.; ASTIA AD 856531.

7. Soland, D.E. et al. Excavation Seismology, Annual Technical Report. Bu Mines Contract No. H0210025. Honeywell Systems and Research Center, St. Paul, Minn. March 1972, 216 pp.

8. Walton, G.G. Three-dimensional Seismic Method. Geophysics, v. 37, No. 3, 1972, pp. 418-430.